

# Diastereomerically Pure 6*R*- and 6*S*-3'-Aza-2'-<sup>18</sup>F-Fluoro-5-Methyltetrahydrofolates Show Unprecedentedly High Uptake in Folate Receptor–Positive KB Tumors

Silvan D. Boss<sup>1</sup>, Cristina Müller<sup>2</sup>, Klaudia Siwowska<sup>2</sup>, Raffaella M. Schmid<sup>2</sup>, Viola Groehn<sup>3</sup>, Roger Schibli<sup>1,2</sup>, and Simon M. Ametamey<sup>1</sup>

<sup>1</sup>Department of Chemistry and Applied Biosciences, Institute of Pharmaceutical Sciences, ETH Zurich, Zurich, Switzerland; <sup>2</sup>Center for Radiopharmaceutical Sciences ETH-PSI-USZ, Paul Scherrer Institut, Villigen-PSI, Switzerland; and <sup>3</sup>Merck & Cie, Schaffhausen, Switzerland

The aim of this study was to develop the radiosyntheses of diastereomerically pure 6*R*- and 6*S*-3'-aza-2'-<sup>18</sup>F-fluoro-5-methyltetrahydrofolate (MTHF) (6*R*-<sup>18</sup>F-**1** and 6*S*-<sup>18</sup>F-**1**) using the integrated approach and to compare the in vitro and in vivo performance characteristics of both radioligands with the previously reported 3'-aza-2'-<sup>18</sup>F-fluorofolic acid tracer (<sup>18</sup>F-**2**), the oxidized form. **Methods:** 6*R*-<sup>18</sup>F-**1**, 6*S*-<sup>18</sup>F-**1**, and <sup>18</sup>F-**2** were radiolabeled with <sup>18</sup>F using aromatic nucleophilic substitution reaction. In vitro cell uptake studies and binding affinity assays were performed using folate receptor (FR)- $\alpha$ -expressing KB cells. PET/CT imaging and biodistribution experiments were performed with KB tumor-bearing mice. **Results:** Reference compounds 6*R*-**1** and 6*S*-**1** were obtained after acidic hydrolysis of the corresponding protected intermediates 6*R*-**3** and 6*S*-**3** in high chemical yields (81%–87%) and chemical purities of more than 95%. 6*R*-<sup>18</sup>F-**1**, 6*S*-<sup>18</sup>F-**1**, and <sup>18</sup>F-**2** were obtained after a 2-step radiosynthetic procedure in a decay-corrected radiochemical yield of up to 5% and molar radioactivities ranging from 20 to 250 GBq/ $\mu$ mol. In vitro binding affinity studies using FR- $\alpha$ -positive KB cells gave half-maximal inhibitory concentrations of 27.1  $\pm$  3.7 and 23.8  $\pm$  4.0 nM for 6*R*-**1** and 6*S*-**1**, respectively, which were higher than for the previously reported 3'-aza-2'-fluorofolic acid **2** (1.4  $\pm$  0.5 nM). Comparably high cell uptake values in FR- $\alpha$ -expressing KB cells were found for all 3 radiofolates. In biodistribution studies, exceptionally high KB tumor uptake value of over 32% injected activity per gram of tissue for both 6*R*-<sup>18</sup>F-**1** and 6*S*-<sup>18</sup>F-**1** was observed at 180 min after injection, whereas for <sup>18</sup>F-**2** only 15% injected activity per gram was found in the KB tumors. Radioactivity uptake in the kidneys, liver, salivary glands, and spleen was substantially different for the 6*R*- and 6*S*-diastereoisomers and <sup>18</sup>F-**2**. Excellent KB tumor visualization was found in PET/CT images with 6*R*-<sup>18</sup>F-**1** and 6*S*-<sup>18</sup>F-**1**, both of which outperformed the corresponding oxidized <sup>18</sup>F-**2**. **Conclusion:** We have successfully radiolabeled 6*R*- and 6*S*-3'-aza-2'-<sup>18</sup>F-fluoro-5-MTHF with <sup>18</sup>F using the integrated approach. Our results suggest that both 6*R*- and 6*S*-3'-aza-2'-<sup>18</sup>F-fluoro-5-MTHF are promising reduced radiofolates for imaging FR- $\alpha$ -expressing cancers.

**Key Words:** folate receptor; 5-methyltetrahydrofolate; <sup>18</sup>F; PET; imaging

**J Nucl Med 2019; 60:135–141**  
DOI: 10.2967/jnumed.118.213314

**T**he folate receptor (FR)- $\alpha$  represents a promising target for tumor imaging since it is overexpressed on various epithelial tumor types such as ovarian, endometrial, renal, breast, lung, and colorectal cancer but shows only limited expression in healthy tissues, primarily in the kidneys (1). In the past 2 decades, a large number of folic acid-based radiopharmaceuticals have been investigated for imaging FR-positive tumor tissues. However, folic acid-based radiotracers seem to have a limitation regarding their uptake into FR-positive tumors given that only slightly increased tumor uptake values were observed when modifications were made to the chemical moieties linked to folic acid (2–5).

Our group was the first to report on the syntheses and biologic evaluation of <sup>18</sup>F-labeled 6*S*- and 6*R*-5-methyltetrahydrofolate (MTHF) conjugates as an alternative to folic acid derivatives for targeting FR-positive tumors (6). The pendant approach, which involves the reaction of a radiolabeled prosthetic group with 5-MTHF, resulting in a radioconjugate, was used for the <sup>18</sup>F labeling of 5-MTHF, and stable radiotracers were obtained in the presence of antioxidants. The biologic results of the study demonstrated differences in the in vivo behavior of the diastereoisomers of 5-MTHF, and the conclusion drawn from that study was that 5-MTHF-based derivatives can be used as alternative targeting molecules to image FR-positive tumor tissues.

Another strategy that can be adapted for the <sup>18</sup>F labeling of folic acid derivatives is the integrated approach, as previously demonstrated by Ross et al. (7). This approach allows the incorporation of the <sup>18</sup>F radiolabel directly into the folic acid-targeting molecule without the need for a prosthetic group and has the further advantage that the obtained folate derivative is structurally close to folic acid. However, it was unclear whether the integrated approach, which involved harsher reaction conditions for the <sup>18</sup>F-incorporation step, could be used for the radiosynthesis of the chemically less stable 5-MTHF derivatives (8–10).

The aim of the present study was to assess in a first step whether the radiosyntheses of 6*R*- and 6*S*-3'-aza-2'-<sup>18</sup>F-fluoro-5-MTHF

Received Apr. 19, 2018; revision accepted Jun. 14, 2018.

For correspondence or reprints contact: Simon M. Ametamey, Radiopharmaceutical Sciences, Institute of Pharmaceutical Sciences, ETH Zurich, Vladimir-Prelog-Weg 4, CH-8093 Zurich.

E-mail: simon.ametamey@pharma.ethz.ch

Published online Jul. 24, 2018.

COPYRIGHT © 2019 by the Society of Nuclear Medicine and Molecular Imaging.

(6*R*-<sup>18</sup>F-**1** and 6*S*-<sup>18</sup>F-**1**, Fig. 1) would be feasible using the integrated approach. In a second step, and more importantly, we aimed to address the question of whether 6*R*- and 6*S*-3'-aza-2'-<sup>18</sup>F-fluoro-5-MTHF would show comparable *in vivo* performance characteristics when compared with the previously reported 3'-aza-2'-<sup>18</sup>F-fluorofolic acid (<sup>18</sup>F-**2**, Fig. 1) (*11*). 6*R*-<sup>18</sup>F-**1** and 6*S*-<sup>18</sup>F-**1** are the corresponding reduced forms of <sup>18</sup>F-**2**, which was synthesized using the integrated approach by our group and is currently being evaluated in a clinical trial.

The results of the study show that the radiolabeling with <sup>18</sup>F of both diastereomers, 6*R*-<sup>18</sup>F-**1** and 6*S*-<sup>18</sup>F-**1**, can be accomplished using the integrated approach. Furthermore, 6*R*-<sup>18</sup>F-**1** and 6*S*-<sup>18</sup>F-**1** outperform <sup>18</sup>F-**2** and show the highest tumor uptake ever obtained for a radiofolate.

## MATERIALS AND METHODS

### General

General information can be found in a previous publication (*6*).

### Chiral High-Performance Liquid Chromatography (HPLC) Separation

The diastereomeric 1:1 mixtures of 6*R*- and 6*S*-*N*<sup>2</sup>-acetyl-3'-aza-2'-chloro-5-MTHF-di-*tert*-butylester (6*R*-**4** and 6*S*-**4**) and 6*R*- and 6*S*-*N*<sup>2</sup>-acetyl-3'-aza-2'-fluoro-5-MTHF-di-*tert*-butylester (6*R*-**3** and 6*S*-**3**) were provided by Merck & Cie (Supplemental Fig. 1; supplemental materials are available at <http://jnm.snmjournals.org>). Then the diastereomers were separated by chiral HPLC using a Reprosil 100 Chiral-NR HPLC column (Dr. Maisch GmbH) running on normal phase (isocratic, hexane/isopropanol 1:1, Supplemental Fig. 2).

### Synthesis of 6*R*- and 6*S*-3'-Aza-2'-Fluoro-5-MTHF

6*R*-**3** (7.00 mg, 11.1 μmol) or 6*S*-**3** (8.00 mg, 12.6 μmol) was dissolved in acetone (200 μL) and 4 M HCl (500 μL) and stirred for 1 h at 70°C. After completion of the reaction, 4 M NaOH (500 μL) was added and the product was purified by semipreparative HPLC. Lyophilization of the product fractions afforded 6*R*-**1** or 6*S*-**1** as white solids in 87% (4.62 mg) and 81% yield (4.96 mg), respectively, in high chemical and diastereomeric purity of more than 95%. 6*R*-**1**: <sup>1</sup>H nuclear MR (500 MHz, D<sub>2</sub>O) δ 7.85 (t, *J* = 8.8 Hz, 1H), 6.39 (d, *J* = 8.8 Hz, 1H), 4.35 (dd, *J* = 8.2, 4.6 Hz, 1H), 3.68 (d, *J* = 13.0 Hz, 1H), 3.64–3.56 (m, 1H), 3.49 (d, *J* = 13.0 Hz, 2H), 3.43–3.32 (m, 1H), 2.86

(s, 3H), 2.42–2.28 (m, 2H), 2.25–2.14 (m, 1H), 2.08–1.99 (m, 1H). High-resolution mass spectrometry (matrix-assisted laser desorption/ionization) calculated for C<sub>19</sub>H<sub>23</sub>FN<sub>8</sub>O<sub>6</sub>: 478.1719; found: 478.1718. 6*S*-**1**: <sup>1</sup>H nuclear MR (500 MHz, D<sub>2</sub>O) δ 7.85 (t, *J* = 8.8 Hz, 1H), 6.39 (d, *J* = 8.8 Hz, 1H), 4.36 (dd, *J* = 8.0, 4.6 Hz, 1H), 3.77–3.62 (m, 2H), 3.58–3.44 (m, 3H), 2.91 (s, 3H), 2.42–2.31 (m, 2H), 2.27–2.15 (m, 1H), 2.09–1.98 (m, 1H). High-resolution mass spectrometry (matrix-assisted laser desorption/ionization) calculated for C<sub>19</sub>H<sub>23</sub>FN<sub>8</sub>O<sub>6</sub>: 478.1719; found: 478.1719.

### Preparation of 6*R*- and 6*S*-3'-Aza-2'-<sup>18</sup>F-Fluoro-5-MTHF

Radiosyntheses of 6*R*- and 6*S*-3'-aza-2'-<sup>18</sup>F-fluoro-5-MTHF were performed in analogy to the radiosynthesis of 3'-aza-2'-<sup>18</sup>F-fluorofolic acid previously described in the literature (*11*). The precursor 6*R*- or 6*S*-*N*<sup>2</sup>-acetyl-3'-aza-2'-chloro-5-MTHF di-*tert*-butylester (6*R*-**4** or 6*S*-**4**, 2.50 mg, 3.85 μmol) was dissolved in anhydrous dimethyl sulfoxide (400 μL) and added to the azeotropically dried <sup>18</sup>F-fluoride-cryptate complex (35–42 GBq) (*11*). The reaction mixture was heated at 150°C for 17 min (Fig. 2). Then, the solution was allowed to cool to 75°C and H<sub>2</sub>O (3 mL) was added. The solution was passed through a Sep-Pak Plus tC18 cartridge (Waters, preconditioned with 5 mL of MeOH, followed by 10 mL of H<sub>2</sub>O) for trapping the intermediate 6*R*-<sup>18</sup>F-**3** or 6*S*-<sup>18</sup>F-**3**. Unreacted <sup>18</sup>F-fluoride was removed by rinsing the cartridge with H<sub>2</sub>O (5 mL). The labeled intermediate 6*R*-<sup>18</sup>F-**3** or 6*S*-<sup>18</sup>F-**3** was eluted by passing MeCN (2 mL) through the cartridge into another sealed Wheaton reactor (3 mL). MeCN was evaporated to near dryness under reduced pressure and a nitrogen stream at 105°C. The protecting groups were cleaved by adding 4 M HCl solution (1 mL) to the reactor and heating for 10 min at 60°C to afford 6*R*-<sup>18</sup>F-**1** or 6*S*-<sup>18</sup>F-**1**. A 10 mM sodium phosphate buffer, pH 7.4, containing a 50 mg/mL solution of Na-(+)-L-ascorbate (1 mL) and 4 M NaOH (0.9 mL) was added for stabilizing the product and for neutralizing the acidic solution, respectively. The product was purified by semipreparative HPLC. The product fraction was collected and passed through a sterile filter into a sterile vial. At the end of synthesis, 350–1,600 MBq (1%–5% decay-corrected radiochemical yield) of the final radiotracers were obtained. Molar activity ranged from 20 to 250 GBq/μmol, and radiochemical purity was greater than 95%.

### Circular Dichroism (CD) Spectroscopy

CD spectra were recorded with a Chirascan-Plus CD spectrometer from AppliedPhotophysics and at a wavelength ranging from 200 to 400 nm. The samples were measured with a concentration of 2 mM in CH<sub>3</sub>OH. Background was corrected using pure CH<sub>3</sub>OH before the experiment.

### Determination of Distribution Coefficient

The shake-flask method was used for the determination of the distribution coefficients (log*D*<sub>7.4</sub>) of 6*R*-<sup>18</sup>F-**1** and 6*S*-<sup>18</sup>F-**1** according to a previously published procedure (*12*).

### In Vitro Binding Affinity

The binding affinities of reference compounds 6*R*-**1** and 6*S*-**1**, 6*R*- and 6*S*-5-MTHF, and folic acid to the FR-α were determined in a competitive *in vitro* binding assay on FR-positive KB cells according to a previously published procedure (*11*). The binding curves are available in the supplemental materials.

### Cell Uptake and Internalization

Cell uptake and internalization experiments were performed with both 6*R*-<sup>18</sup>F-**1** or 6*S*-<sup>18</sup>F-**1** as previously described (*13,14*).

### Preparation of Tumor Mice

Animal experiments were performed in compliance with Swiss and local laws on animal protection and approved by the Veterinary Office

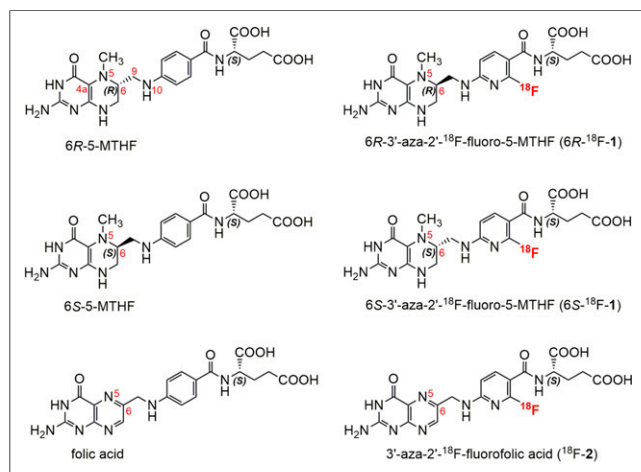


**FIGURE 1.** Chemical structures of 6*R*-5-MTHF, 6*S*-5-MTHF, folic acid, 6*R*-3'-aza-2'-<sup>18</sup>F-fluoro-5-MTHF, 6*S*-3'-aza-2'-<sup>18</sup>F-fluoro-5-MTHF, and 3'-aza-2'-<sup>18</sup>F-fluorofolic acid.

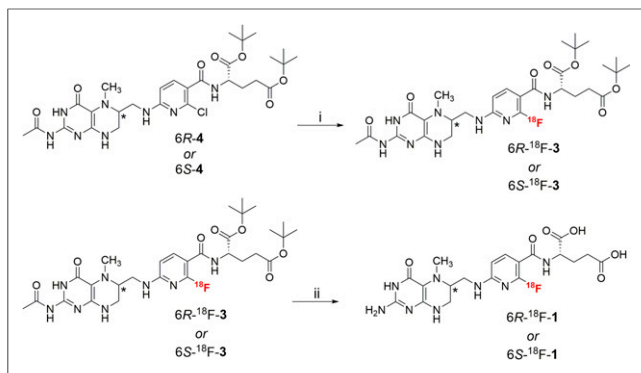


**FIGURE 2.** Two-step radiosynthesis of 6*R*- and 6*S*-<sup>18</sup>F-1<sup>a</sup>. (i) <sup>18</sup>F-CsF-K<sub>2,2,2</sub>, dimethyl sulfoxide (DMSO), 150°C, 17 min. (ii) 4 M HCl, 60°C, 10 min.

of Switzerland. Female CD-1 nude mice were purchased from Charles River and kept on a folate-deficient rodent diet (ssniff Spezialdiäten GmbH) starting 1 wk before the KB tumor cell inoculation. Experiments were performed 2 wk after the KB tumor cell inoculation. A cell suspension ( $5 \times 10^6$  cells in 100  $\mu$ L of phosphate-buffered saline, pH 7.4) was inoculated into the subcutis of each shoulder.

### Biodistribution Studies

Animals were injected with approximately 5 MBq ( $\sim 0.2$  nmol, 100  $\mu$ L) of the corresponding radiotracer via a lateral tail vein ( $n = 4$  per time point). Blocking studies ( $n = 3$ ) were performed with excess folic acid dissolved in phosphate-buffered saline, pH 7.4 (1 mg/mL), which was intravenously injected (100  $\mu$ L per mouse) 2–3 min before injection of the radiotracer. Animals were sacrificed at 0.5, 1, 1.5, 2, and 3 h after injection. Organs and tissues were collected and measured in a  $\gamma$ -counter. The radioactivity that accumulated in organs and tissues was expressed as percentage injected activity per gram of tissue (%IA/g) and decay-corrected.

### PET/CT Imaging Studies

PET/CT scans were performed using a small-animal benchtop PET/CT scanner (G8; Perkin Elmer). The energy window was set to 150–650 keV. Mice were injected intravenously with the <sup>18</sup>F radiotracers ( $\sim 5$  MBq in 100  $\mu$ L,  $\sim 0.2$ – $0.3$  nmol). For blocking studies, an excess of folic acid in phosphate buffered saline (100  $\mu$ g/100  $\mu$ L) was injected 2–3 min before the injection of the radiotracers.

During the scans, which lasted 10 min, the mice were anesthetized using a mixture of isoflurane and oxygen. Scans were performed at 1, 2, and 3 h after injection of the <sup>18</sup>F radiotracers using G8 acquisition software (version 2.0.0.10). The PET scans were followed by a CT scan of 1.5 min. The images were reconstructed with maximum-likelihood expectation maximization using the software of the scanner. All images were prepared using VivoQuant postprocessing software (version 2.10; inviCRO Imaging Services and Software). A Gauss post-reconstruction filter (full width at half maximum, 1 mm) was applied to the images. For presenting the PET/CT images, the scale of the images was adjusted allowing optimal visualization of the tumor tissue and kidneys.

### Metabolite Studies

6*R*-<sup>18</sup>F-1 or 6*S*-<sup>18</sup>F-1 (56.8–62.2 MBq;  $\sim 2.1$ – $3.5$  nmol) was injected intravenously into mice, and the animals were sacrificed 30 min after injection of the radiotracer. Blood, liver, and urine were collected and analyzed. Ice-cold methanol containing a 10 mg/mL concentration of 2-mercaptoethanol and 0.025% (v/v) ammonium hydroxide was added to the blood plasma, homogenized liver, and urine to precipitate the

proteins (15). After centrifugation at 5,000g for 5 min at 4°C, the supernatants of the blood plasma, liver, and urine samples were analyzed by radio-ultra-performance liquid chromatography.

## RESULTS

### Synthesis of Nonradioactive Reference Compounds

Pure diastereomeric 6*R*-3 and 6*S*-3 were obtained after chiral separation and used as starting materials for the synthesis of 6*R*-1 and 6*S*-1. Acidic deprotection of 6*R*-3 and 6*S*-3 in acetone and purification afforded 6*R*- and 6*S*-3'-aza-2'-fluoro-5-MTHF in chemical yields of 81% and 87%, respectively (Fig. 3).

### Determination of the Absolute Configuration of the 2 Reference Diastereoisomers 6*R*-1 and 6*S*-1 by CD

CD spectra of 6*R*- and 6*S*-5-MTHF (Supplemental Fig. 3A) and the 2 diastereomeric pure reference compounds 6*R*- and 6*S*-3'-aza-2'-fluoro-5-MTHF (6*R*-1 and 6*S*-1, Supplemental Fig. 3B) were measured from 200 to 400 nm (16). The resulting spectra of 6*R*- and 6*S*-5-MTHF served as reference spectra, since the stereochemistry of these 2 folates at position 6 of the pterin entity is known. Pterin was reported to have 2 typical absorption bands at around 280 nm and at 345 nm (8,17,18). In all 4 recorded CD spectra, these 2 typical absorption bands were apparent. Correlation of the elution profile and the reference CD spectra of 6*R*- and 6*S*-5-MTHF showed that the *R*-isomers were the first to elute from the chiral column and showed negative and positive peaks at 280 and 310 nm, respectively (Supplemental Fig. 3C). The *S*-isomer eluted second and exhibited positive and negative peaks at 280 and 310 nm (Supplemental Fig. 3D). The same correlation was done with 6*S*-5-MTHF whereby the *S*-diastereomer eluted as the second peak from the chiral HPLC column. As depicted in Supplemental Fig. 3D, the peak at 280 nm was positive and the peak at 310 nm was negative for both folate derivatives. On the basis of these results, we unambiguously determined the absolute configurations of 6*R*- and 6*S*-3'-aza-2'-fluoro-5-MTHF.

### Radiochemistry

6*R*- and 6*S*-<sup>18</sup>F-1 were radiosynthesized in a 2-step reaction sequence starting from the diastereomerically pure chlorinated precursors 6*R*-4 or 6*S*-4 (Fig. 2) obtained via normal-phase chiral HPLC. The reaction sequence involved a nucleophilic aromatic substitution of the chloro leaving group by <sup>18</sup>F-fluoride followed by cleavage of the protecting groups under acidic conditions. After semipreparative HPLC, the radiolabeled diastereoisomers 6*R*-<sup>18</sup>F-1 and 6*S*-<sup>18</sup>F-1 were obtained in a total synthesis time of 100 min, decay-corrected radiochemical yields of 1%–5%, and radiochemical purities of more than 95% with molar radioactivities ranging from

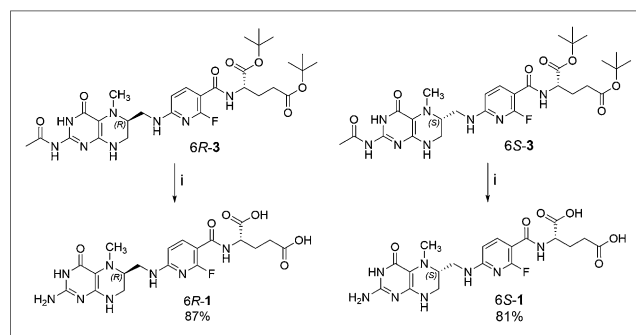


**FIGURE 3.** Synthesis of 6*R*-1 and 6*S*-1<sup>a</sup>. (i) 4 M HCl, acetone, 70°C, 1 h.

20 to 250 GBq/ $\mu\text{mol}$ . Coinjection of the nonradioactive reference compound **6R-1** or **6S-1** confirmed the identity of **6R-<sup>18</sup>F-1** and **6S-<sup>18</sup>F-1**. The distribution coefficient ( $\log D_{7.4}$ ) of both **6R-<sup>18</sup>F-1** and **6S-<sup>18</sup>F-1** was  $-4.8 \pm 0.1$  ( $n = 3$ ), which is in the same range as the  $\log D_{7.4}$  value,  $-4.2 \pm 0.1$ , for **<sup>18</sup>F-2** (11).

### In Vitro Characterization

The binding affinities of the nonradioactive reference compounds **6R-1**, **6S-1**, and **2** to the FR- $\alpha$  was determined in a displacement assay with <sup>3</sup>H-folic acid using KB tumor cells. The binding curves are available in the supplemental materials. The two reduced aza-folates **6R-1** and **6S-1** exhibited affinities that were similar to FR- $\alpha$  and comparable to **6R-5-MTHF**s and **6S-5-MTHF**s (Table 1). The half-maximal inhibitory concentration values of 3'-aza-2'-fluorofolic acid **2** and folic acid were considerably higher than those of the 5-MTHF compounds.

### Cell Uptake and Internalization with KB Cells

Cell uptake and internalization of **6R-<sup>18</sup>F-1**, **6S-<sup>18</sup>F-1**, and **<sup>18</sup>F-2** were investigated using FR- $\alpha$ -expressing KB cells (Fig. 4). A constant increase in cell uptake over time was observed for all radiofolates, resulting in a similar uptake in the range of 50%–60% of total added radioactivity after 3 h of incubation at 37°C. The internalized fraction was 22% of total added activity for **<sup>18</sup>F-2**, whereas 16% and 8% were internalized for **6S-<sup>18</sup>F-1** and **6R-<sup>18</sup>F-1**, respectively. FR- $\alpha$ -specific binding was confirmed by coincubating cells with the radiotracer and an excess of folic acid, resulting in a high inhibition of uptake to less than 1% for all 3 radiofolates.

### Biodistribution

Biodistribution studies were performed with KB tumor-bearing mice at different time points after injection of **6R-<sup>18</sup>F-1**, **6S-<sup>18</sup>F-1**, or **<sup>18</sup>F-2**, and the results are summarized in Figures 5 and 6 and Supplemental Tables 1–3.

A high tumor uptake of  $13.3 \pm 1.80$  %IA/g for **6R-<sup>18</sup>F-1** and  $11.13 \pm 0.90$  %IA/g for **6S-<sup>18</sup>F-1** was already observed at 0.5 h after injection (Fig. 5). Tumor uptake constantly increased over time, resulting in exceptionally high values of  $32.3 \pm 6.1$  %IA/g for **6R-<sup>18</sup>F-1** and  $34.8 \pm 6.0$  %IA/g for **6S-<sup>18</sup>F-1** at 3 h after injection. In contrast, tumor uptake of **<sup>18</sup>F-2** increased only slightly over time to only half the amount of radioactivity ( $15.0 \pm 2.3$  %IA/g) of the reduced folates. Injection of folic acid reduced the uptake in the tumors by 85 and 89 %IA/g for the **6R-** and **6S-**isomers, respectively, and by 80 %IA/g for **<sup>18</sup>F-2** at 1 h after

TABLE 1

Comparison of In Vitro Binding Affinities of **6R-1**, **6S-1** and **2** in Comparison to **6R-5-MTHF** and **6S-5-MTHF** and Folic Acid to FR- $\alpha$  ( $n = 3$ )

Compound	IC <sub>50</sub> (nM)
<b>6R-1</b>	27.1 $\pm$ 3.7
<b>6S-1</b>	23.8 $\pm$ 4.0
<b>2</b>	1.4 $\pm$ 0.5
<b>6R-5-MTHF</b>	25.8 $\pm$ 5.8
<b>6S-5-MTHF</b>	20.6 $\pm$ 0.4
Folic acid	0.4 $\pm$ <0.1

IC<sub>50</sub> = half-maximal inhibitory concentration.

Binding curves are available in the supplemental materials.

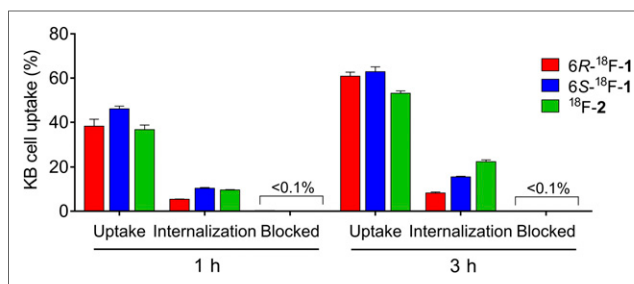


FIGURE 4. Cell uptake and internalization of **6R-<sup>18</sup>F-1**, **6S-<sup>18</sup>F-1**, and **<sup>18</sup>F-2** with FR- $\alpha$ -expressing KB cells incubated at 37°C for 1 or 3 h. Cell uptake was calculated for 0.3 mg of protein. Blocking studies were performed using excess of folic acid.

injection. Kidney uptake was already lowest for **6R-<sup>18</sup>F-1** at 0.5 h after injection and considerably decreased over time to below 20 %IA/g. In contrast, radioactivity accumulation in the kidneys was nearly constant for **6S-<sup>18</sup>F-1** and **<sup>18</sup>F-2** over the investigated 3 h. Liver uptake was 2- and 3-fold higher for **6R-<sup>18</sup>F-1** than for **<sup>18</sup>F-2** and **6S-<sup>18</sup>F-1**, respectively, and was constant over time for all

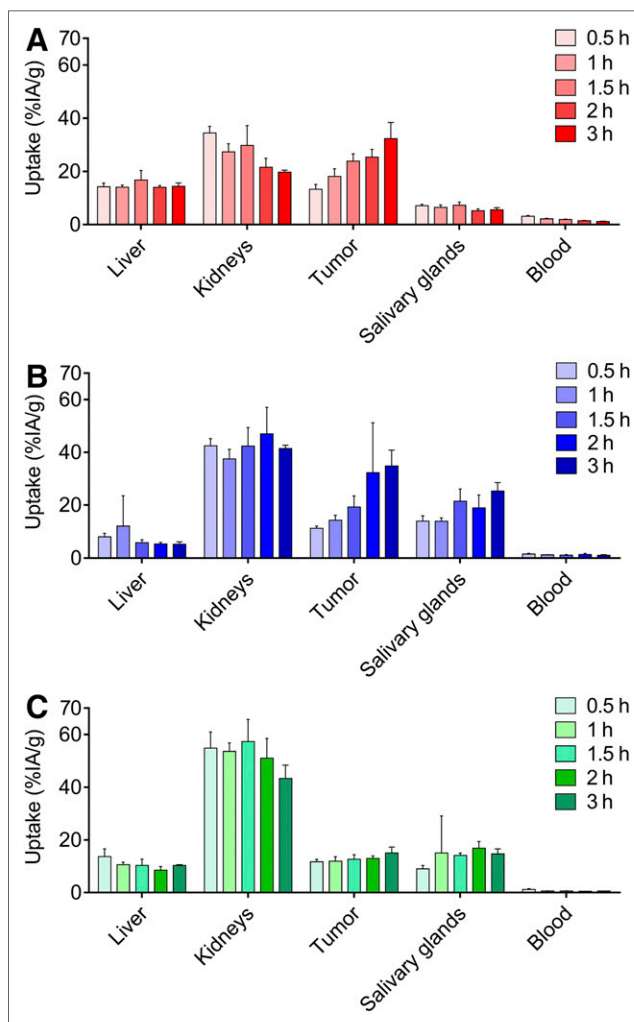
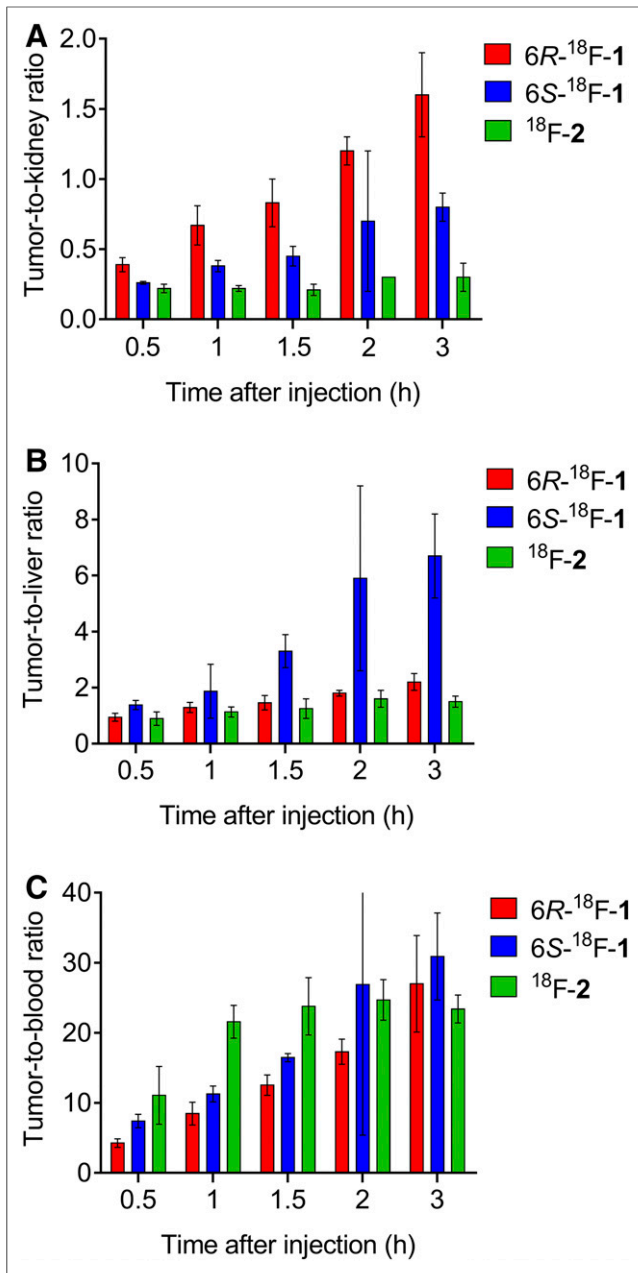


FIGURE 5. Radioactivity accumulation of **6R-<sup>18</sup>F-1** (A), **6S-<sup>18</sup>F-1** (B), and **<sup>18</sup>F-2** (C) in some selected tissues at 0.5, 1, 1.5, 2, and 3 h after injection.



**FIGURE 6.** Comparison of tumor-to-kidney (A), tumor-to-liver (B), and tumor-to-blood (C) ratios of 6R-<sup>18</sup>F-1, 6S-<sup>18</sup>F-1, and <sup>18</sup>F-2 at all investigated time points.

radiofolates. Liver uptake could not be blocked with folic acid for any of the 3 radiofolates, suggesting unspecific uptake. FR- $\alpha$ -specific salivary gland uptake was approximately 3-fold higher for 6S-<sup>18</sup>F-1 and <sup>18</sup>F-2 than for 6R-<sup>18</sup>F-1.

6R-<sup>18</sup>F-1 exhibited the highest tumor-to-kidney ratio of the 3 radiofolates at all investigated time points because of the decreased kidney uptake (Fig. 6). An exceptionally high tumor-to-kidney ratio of  $1.63 \pm 0.32$  was determined for 6R-<sup>18</sup>F-1 at 3 h after injection. The tumor-to-liver ratio was the highest for 6S-<sup>18</sup>F-1, as can be explained by the decreased liver uptake. The tumor-to-blood ratios constantly increased over time for all 3 radiofolates, resulting in similar values 3 h after injection.

### In Vivo PET Imaging

PET/CT scans of KB tumor-bearing mice were performed at 1 and 3 h after injection of 6R-<sup>18</sup>F-1, 6S-<sup>18</sup>F-1, or <sup>18</sup>F-2 (Fig. 7). A considerably higher uptake of both reduced radiotracers was already observed in KB tumor xenografts 1 h after injection and the tumors were well visualized 3 h after injection for both 6R-<sup>18</sup>F-1 and 6S-<sup>18</sup>F-1. FR-positive kidneys were clearly visualized 1 h after injection with 6R-<sup>18</sup>F-1 but nearly invisible 3 h after injection. In contrast, high kidney accumulation was observed for 6S-<sup>18</sup>F-1 and <sup>18</sup>F-2 at all investigated time points. Radioactivity uptake in the liver was found mainly for <sup>18</sup>F-2 and the 6R-isomer; however, after 3 h after injection the liver was only barely visible for both radiotracers. Radioactivity uptake in the salivary glands, gallbladder, and choroid plexus was higher for the 6S-isomer than for the 6R-isomer. Blocking studies were performed by injecting an

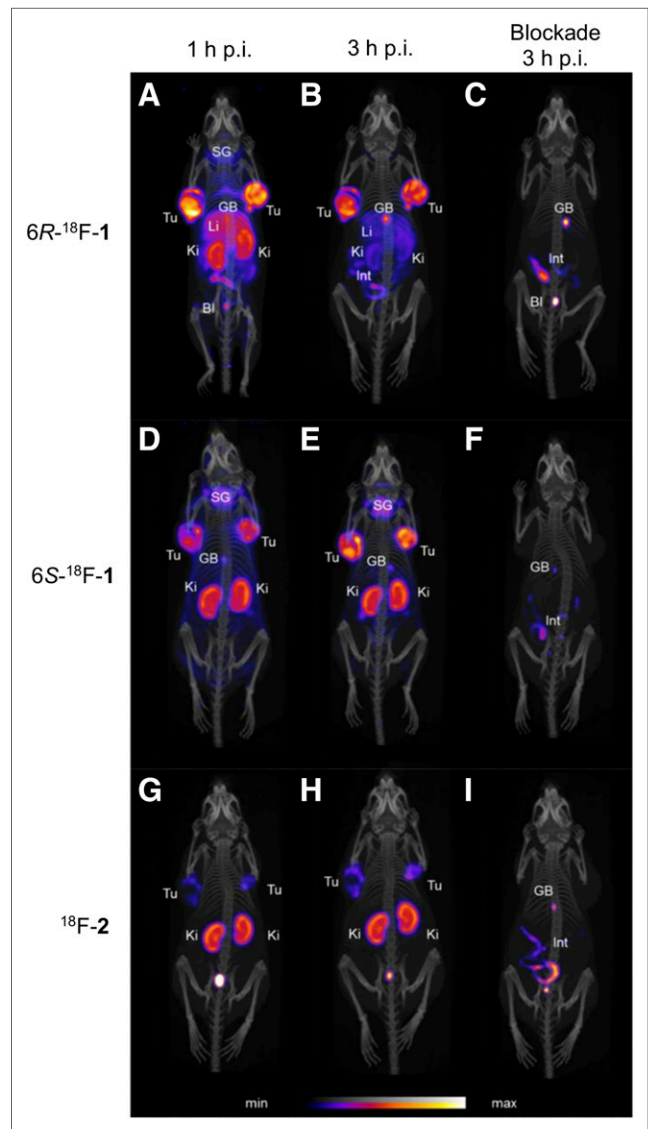


**FIGURE 7.** PET/CT scans of KB tumor-bearing mouse injected with 6R-<sup>18</sup>F-1 (A–C), 6S-<sup>18</sup>F-1 (D–F), and <sup>18</sup>F-2 (G–I) at 1 and 3 h after injection and blocking at 3 h after injection. Tu = KB tumor; Li = liver; Ki = kidney; SG = salivary glands; GB = gallbladder; BI = urinary bladder; Int = intestine/feces.

excess of folic acid before administration of the radiotracers and resulted in a remarkably reduced uptake of 6R-<sup>18</sup>F-1, 6S-<sup>18</sup>F-1, and <sup>18</sup>F-2 in all FR-positive tissues (KB tumor xenografts, kidneys, salivary glands, and choroid plexus).

### Metabolite Studies

The in vivo stability experiments revealed no radiometabolites in blood plasma, urine, or liver samples for either radiofolate. Only intact parent radiotracers were detected. The same finding was previously reported for the oxidized version of <sup>18</sup>F-2 (11).

## DISCUSSION

The nonradioactive reference compounds 6R-1 and 6S-1 could not be separated on either a normal C18 or a chiral HPLC column; therefore, the 6R- and 6S-diastereoisomers were separated using the protected intermediates 6R-3 and 6S-3, as these were well separated on the chiral HPLC column. After acidic deprotection of the protecting groups of 6R-3 and 6S-3, elucidation and assignment of the absolute configuration of the nonradioactive reference compounds 6R-1 and 6S-1 were performed using CD spectroscopy.

6R-1 and 6S-1 showed similar IC<sub>50</sub> values to the FR-α as did the nonderivatized 6R- and 6S-5-MTHF, indicating that modifications on the pteroyl moiety have no influence on the binding affinity to the FR-α (Table 1). The half-maximal inhibitory concentrations for compound 2 and folic acid were considerably lower than those for the 5-MTHF derivatives and agreed with values reported in the literature (18).

The radiosynthesis of 6R-<sup>18</sup>F-1 and 6S-<sup>18</sup>F-1 via the integrated approach was accomplished using a 2-step synthetic procedure starting with the protected chlorinated, diastereomerically pure precursor 6R-4 or 6S-4, which were obtained after chiral HPLC separation of the diastereomeric 1:1 mixture. The varying radiochemical yield of 6R-<sup>18</sup>F-1 and 6S-<sup>18</sup>F-1 can be explained by the aromatic substitution reaction, which was found to be very water-sensitive. However, a critical issue during the radiosynthesis was the chemical stability of the radiolabeled reduced folate derivatives, similar to the findings for the previously reported <sup>18</sup>F-labeled 5-MTHF conjugates (6). High chemical decomposition of 6R-<sup>18</sup>F-1 and 6S-<sup>18</sup>F-1 was observed during the radiolabeling, especially after the cleavage of the protecting groups. This chemical instability of the 3'-aza-5-MTHF tracers was revealed as a major disadvantage compared with the corresponding folic acid product, <sup>18</sup>F-2, which was stable under the same reaction conditions. However, in the presence of the antioxidant sodium ascorbate, 6R-<sup>18</sup>F-1 and 6S-<sup>18</sup>F-1 were found to be stable over 3 h after isolation. No additional thiol-bearing antioxidant was required for stabilization as opposed to <sup>18</sup>F-labeled 5-MTHF conjugates, where a combination of both sodium ascorbate and L-cysteine was crucial for their stabilization (6). Optimization of the reaction conditions has been planned for the future. The high variation of the molar activity can be explained by the challenging separation of the final radioproduct and the chlorinated side-product.

Cell experiments with FR-α-expressing KB cells revealed high specific uptake and internalization of all 3 aza-folate radiotracers, suggesting that the lower binding affinity of the 5-MTHF derivatives has no influence on the binding to FR-α (Fig. 4).

6R-<sup>18</sup>F-1 and 6S-<sup>18</sup>F-1 showed high in vivo stability, which was critical for in vivo experiments, including biodistribution and PET studies. Because 5-MTHF is the predominant folate circulating in the body, accounting for approximately 98% of folates in human plasma, high in vivo stability was expected (15). In biodistribution studies, both 6R-<sup>18</sup>F-1 and 6S-<sup>18</sup>F-1 showed exceptionally high KB

tumor uptake of over 32 %IA/g at 180 min after injection, representing the highest tumor uptake value for a folate-based radiopharmaceutical ever reported in the literature (Supplemental Tables 1 and 2). Excellent tumor visualization for 6R-<sup>18</sup>F-1 and 6S-<sup>18</sup>F-1 was also evident in the PET imaging studies, whereas background activity was low, suggesting that the 3'-aza-5-MTHF tracers were not transported by the ubiquitously expressed reduced folate carrier (19). For <sup>18</sup>F-2, only 15 %IA/g was found in the tumors, resulting in a poor visualization of the tumors in the PET images compared with both reduced radiofolates (Fig. 7). A surprising finding of this study was that the accumulation of 6R-<sup>18</sup>F-1 and 6S-<sup>18</sup>F-1 in the KB tumor xenografts considerably increased over time, whereas for <sup>18</sup>F-2 the uptake was nearly constant over time (Fig. 5). This was not the case for <sup>18</sup>F-2, as radioactivity uptake in the kidneys and liver was nearly constant over time. The different binding affinities of the 5-MTHF and the folic acid derivatives to the FR, or different transport characteristics by other transporters expressed in the kidneys and the liver, could be a potential reason for these considerable differences in radioactivity accumulation. However, further experiments are needed to investigate the transport characteristics of the aza-folates. 6R-<sup>18</sup>F-1 exhibited the highest tumor-to-kidney ratio (1.63) of all 3 radiofolates because of its low kidney uptake—a major advantage compared with the folic acid-based radiotracer (0.35). Low kidney uptake of 6R-<sup>18</sup>F-1 was also visible in the PET images, suggesting a fast washout from the kidneys. In contrast, liver uptake was higher for 6R-<sup>18</sup>F-1 than for 6S-<sup>18</sup>F-1 or <sup>18</sup>F-2, and these results agreed with the PET images. A possible explanation might be the higher hepatobiliary clearance of the R-isomer than the S-isomer or <sup>18</sup>F-2. From an imaging point of view, the lower uptake of the S-isomer in the liver is advantageous because it would permit imaging of FR-positive tumors near the liver.

## CONCLUSION

In this study, we showed that 6R-<sup>18</sup>F-1 and 6S-<sup>18</sup>F-1 can be directly radiolabeled with <sup>18</sup>F using the integrated approach. Both <sup>18</sup>F-labeled 5-MTHF derivatives exhibited a tumor uptake of over 32 %IA/g, which is the highest tumor uptake ever obtained for a radiofolate. These results demonstrate that both 6R- and 6S-3'-aza-2'-<sup>18</sup>F-fluoro-5-MTHF are highly promising radiopharmaceuticals for clinical trials to image FR-α-positive tumors.

## DISCLOSURE

This project was financially supported by Merck & Cie (Schaffhausen, Switzerland) and by the Swiss National Science Foundation (grant 310030\_156803). No other potential conflict of interest relevant to this article was reported.

## ACKNOWLEDGMENTS

We thank Susan Cohrs, Claudia Keller, Bruno Mancosu, Patrycja Guzik, and Jasmin Egli for their support and technical assistance.

## REFERENCES

1. Parker N, Turk MJ, Westrick E, Lewis JD, Low PS, Leamon CP. Folate receptor expression in carcinomas and normal tissues determined by a quantitative radioligand binding assay. *Anal Biochem*. 2005;338:284–293.
2. Low PS, Henne W, Doorneweerd D. Discovery and development of folic-acid-based receptor targeting for imaging and therapy of cancer and inflammatory diseases. *Acc Chem Res*. 2008;41:120–129.

3. Low PS, Kularatne SA. Folate-targeted therapeutic and imaging agents for cancer. *Curr Opin Chem Biol.* 2009;13:256–262.
4. Müller C. Folate-based radiotracers for PET imaging: update and perspectives. *Molecules.* 2013;18:5005–5031.
5. Siwowska K, Haller S, Bortoli F, et al. Preclinical comparison of albumin-binding radiofolates: impact of linker entities on the in vitro and in vivo properties. *Mol Pharm.* 2017;14:523–532.
6. Boss SD, Müller C, Siwowska K, et al. Reduced <sup>18</sup>F-folate conjugates as a new class of PET tracers for folate receptor imaging. *Bioconjug Chem.* 2018;29:1119–1130.
7. Ross TL, Müller C, Groehn V, Schibli R, Ametamey SM. A new <sup>18</sup>F-labeled folic acid derivative with improved properties for the PET imaging of folate receptor-positive tumors. *J Nucl Med.* 2010;51:1756–1762.
8. Juzeniene A, Tam TTT, Iani V, Moan J. 5-methyltetrahydrofolate can be photo-degraded by endogenous photosensitizers. *Free Radic Biol Med.* 2009;47:1199–1204.
9. Steindal AH, Juzeniene A, Johnsson A, Moan J. Photodegradation of 5-methyl-tetrahydrofolate: biophysical aspects. *Photochem Photobiol.* 2006;82:1651–1655.
10. Blair JA, Pearson AJ, Robb AJ. Autooxidation of 5-methyl-5,6,7,8-tetrahydro-folic acid. *J Chem Soc Perkin Trans 2.* 1975;6:18–21.
11. Betzel T, Müller C, Groehn V, et al. Radiosynthesis and preclinical evaluation of 3'-aza-2'-[<sup>18</sup>F]fluorofolic acid: a novel PET radiotracer for folate receptor target-ing. *Bioconjug Chem.* 2013;24:205–214.
12. Wilson AA, Jin L, Garcia A, DaSilva JN, Houle S. An admonition when mea-suring the lipophilicity of radiotracers using counting techniques. *Appl Radiat Isot.* 2001;54:203–208.
13. Müller C, Mindt TL, de Jong M, Schibli R. Evaluation of a novel radiofolate in tumour-bearing mice: promising prospects for folate-based radionuclide therapy. *Eur J Nucl Med Mol Imaging.* 2009;36:938–946.
14. Ladino CA, Chari, Ravi VJ, Bourret L, Kedersha NL, Goldmacher VS. Folate-maytansinoids: target-selective drugs of low molecular weight. *Int J Cancer.* 1997;73:859–864.
15. Zheng X-H, Jiang L-Y, Zhao L-T, Zhang Q-Y, Ding L. Simultaneous quanti-tation of folic acid and 5-methyltetrahydrofolic acid in human plasma by HPLC–MS/MS and its application to a pharmacokinetic study. *J Pharm Anal.* 2015;5:269–275.
16. Berova N, Di Bari L, Pescitelli G. Application of electronic circular dichroism in configurational and conformational analysis of organic compounds. *Chem Soc Rev.* 2007;36:914–931.
17. Petroselli G, Erra-Balsells R, Cabrerizo FM, et al. Photosensitization of 2'-deox-yadenosine-5'-monophosphate by pterin. *Org Biomol Chem.* 2007;5:2792–2799.
18. Wang X, Shen F, Freisheim JH, Gentry LE, Ratnam M. Differential stereospec-ificities and affinities of folate receptor isoforms for folate compounds and anti-folates. *Biochem Pharmacol.* 1992;44:1898–1901.
19. Fowler B. The folate cycle and disease in humans. *Kidney Int Suppl.* 2001;78: S221–S229.

### Erratum

In “Characterization of 3 Novel Tau Radiopharmaceuticals, <sup>11</sup>C-RO-963, <sup>11</sup>C-RO-643, and <sup>18</sup>F-RO-948, in Healthy Controls and in Alzheimer Subjects,” by Wong et al. (*J Nucl Med.* 2018;59:1869–1876), the indicated affiliations for Susan Resnick and Esther Oh are incorrect. The correct affiliations should be *Susan Resnick<sup>6</sup>, Lab of Behavioral Neuroscience, NIH-NIA IRP, Baltimore, Maryland;* and *Esther Oh<sup>7</sup>, Department of Medicine, Johns Hopkins University, Baltimore, Maryland.* In addition, affiliation 1 should read Section of High Resolution Brain PET, *Department of Radiology and Radiological Sciences, Division of Nuclear Medicine, Johns Hopkins University, Baltimore, Maryland.* In the Key Words, “tau radiopharmaceuticals” was inadvertently left out of the list. Finally, the last name of one of the authors was misspelled. “Abhay Mogekar” should be “Abhay Moghekar.” We regret these errors.